physica status solidi a
www.pss-a.com

Intrinsic Amorphous Silicon Bilayers for Effective Surface Passivation in Silicon Heterojunction Solar Cells: A Comparative Study of Interfacial Layers

Hitoshi Sai, Hung-Jung Hsu, Po-Wei Chen, Pei-Ling Chen, and Takuya Matsui*

The impact of intrinsic amorphous silicon bilayers in amorphous silicon/crystalline silicon (a-Si:H/c-Si) heterojunction solar cells is investigated. Intrinsic a-Si:H films with a wide range of film densities and hydrogen contents are prepared via a plasma-enhanced chemical vapor deposition (PECVD) technique by modifying various process parameters. For silicon heterojunction (SHJ) solar cells with a-Si:H films applied as single i-layers, the resulting surface passivation at the a-Si:H/c-Si interface is poor. However, surface passivation is significantly improved by applying intrinsic bilayers, which are composed of a porous interfacial layer (≈2 nm) and an overlying dense layer (≈8 nm). The microstructure factor *R of the interfacial a-Si:H layer, which is related to the Si—H bond microstructure and determined by infrared absorption spectroscopy, closely correlates to the surface passivation capability of the bilayers. A variety of PECVD process parameters (temperature, pressure, or precursor gas species) can be utilized to grow an interfacial layer for good surface passivation, provided that its *R** is controlled within a suitable range. This indicates that *R** is a key universal parameter for optimizing i-bilayers and realizing high-efficiency SHJ solar cells.**

1. Introduction

In general, surface passivation is crucial to realize high-efficiency crystalline silicon (c-Si) solar cells. One of the best materials for this purpose is hydrogenated amorphous silicon (a-Si:H), which is grown by plasma-enhanced chemical vapor deposition (PECVD) or hot-wire CVD (HWCVD, also called "catalytic CVD") at low temperature (<250 °C). The superior passivation ability of a-Si:H has been successfully demonstrated in a-Si:H/c-Si heterojunction (SHJ) solar cells[1,2] with high open circuit voltages (V_{OC}) and conversion efficiencies >25% in either both-side contact cells[3,4] or back contact cells.[5,6] In addition, the SHJ architecture is suited to very thin c-Si cells, in which surface recombination plays a more critical role.[7–10] Moreover, SHJ solar cells exhibit lower temperature coefficients than the conventional homojunction ones due to their high V_{OC}, and therefore a higher energy yield is obtained in outdoor operation.[11–13]

The key enabler of high-efficiency SHJ solar cells is an intrinsic (i) a-Si:H layer inserted between a c-Si wafer and an overlying doped a-Si:H layer, which results in excellent surface passivation at the a-Si:H/c-Si interface.[1,14,15] The growth condition of the i-layer has to be controlled carefully for preventing epitaxial growth at the a-Si:H/c-Si interface, which is generally detrimental for surface passivation.[16–18] To this end, interfacial layers such as porous (underdense) a-Si:H layers,[4,19–21] a-Si:H alloys, including amorphous silicon oxides and carbides (a-SiO_X:H[22,23] and a-SiC_X:H[24]), and very thin oxides[25,26] have been investigated. In addition, hydrogen dilution of SiH_4 plasma[18,27,28]has a significant impact on the surface passivation. Furthermore, surface passivation at the a-Si:H/c-Si interface is strongly affected also by overlying doped (p- or n-type) layers, which are necessary for collection of either electrons or holes.[19,29,30]

Recently, we reported that good surface passivation at the a-Si:H/c-Si interface can be realized by using an intrinsic a-Si:H bilayer, i.e., a stack consisting of a porous interfacial layer and an additional dense layer.[21] This bilayer approach is particularly effective in maintaining surface passivation after the deposition of an overlying p-layer. We found that the quality of surface passivation shows a good correlation with the microstructure factor *R** of the interfacial a-Si:H layer, which is related to the Si—H bond microstructure within the a-Si:H network.[31] The effectiveness of the bilayer approach was also demonstrated very recently by Ru et al. with the record efficiency of 25.11% in a full-size bifacial SHJ solar cell.[4]

The purpose of this study is to obtain a more general insight on the effectiveness of an intrinsic a-Si:H bilayer on SHJ solar cell performance, with a particular focus on the correlation between the growth condition and the material properties of the interfacial a-Si:H layer. In this work, we process a-Si:H i-layers by means of PECVD under a wide range of substrate temperatures and gas pressures. Moreover, the effect of

Dr. H. Sai, Dr. T. Matsui
Global Zero Emission Research Center (GZR)
National Institute of Advanced Industrial Science and Technology (AIST)
Tsukuba, Ibaraki 305-8568, Japan
E-mail: hitoshi-sai@aist.go.jp

Dr. H.-J. Hsu, Dr. P.-W. Chen, Dr. P.-L. Chen
Department of Photonics
College of Electrical and Computer Engineering
National Chiao Tung University (NCTU)
Hsinchu 300, Taiwan

The ORCID identification number(s) for the author(s) of this article can be found under https://doi.org/10.1002/pssa.202000743.

DOI: 10.1002/pssa.202000743

precursor gas species is also investigated by introducing disilane (Si_2H_6) in addition to standard monosilane (SiH_4). The optical properties and the Si—H bond microstructure in thin a-Si:H layers are characterized by spectroscopic ellipsometry (SE) and Fourier transform infrared spectroscopy (FT-IR). These a-Si:H layers are applied to SHJ solar cells in the manner of intrinsic single layers and interfacial layers in the bilayer configuration. The surface passivation capability of these films is characterized by measuring minority carrier lifetimes. SHJ solar cells using these i-layers are also fabricated and characterized in terms of not only surface passivation but also photoconversion efficiency.

2. Experimental Section

2.1. Preparation and Characterization of a-Si:H Layers

Intrinsic a-Si:H layers were prepared by means of a PECVD process based on 13.56 MHz capacitively coupled discharge in a parallel plate configuration under a wide range of substrate temperatures (T_S), gas pressures (P), and concentrations of Si_2H_6 gas with respect to the total Si precursors (C_{Si2H6}). In general, the a-Si:H films from the Si_2H_6 precursor exhibit a higher deposition rate (DR) and a wider bandgap than those from SiH_4 because dimeric radicals (Si_2H_y) are preferably generated and contribute to the a-Si:H growth process.[32,33] The detailed PECVD conditions for the growth of a-Si:H films are listed in **Table 1**.

For material characterization, a series of thin a-Si:H i-layers (≈10 nm) was deposited on both sides of float-zone (FZ)-grown double-side polished wafers (>1000 Ω cm). The thickness and DR of the i-layers were determined by SE. Optical properties including the bandgap E_g (Tauc gap) and the refractive index were also determined by SE, under the assumption of the Tauc–Lorentz model. In this study, the refractive index at 1 eV (n_1) was characterized as a measure of the film density. The Si—H bond microstructure in these samples was analyzed by a Thermo Fisher iS50 FT-IR spectrometer with N_2 purging. All the spectra were collected in transmission mode with the beam perpendicular to the film surface. The signal-to-noise ratio in the FT-IR spectra of such thin a-Si:H layers was improved by depositing the same films on both sides of the wafer. As mentioned later, the microstructure factor (R^*) and the hydrogen content (C_H) within a-Si:H layers were determined based on the absorption spectra measured with FT-IR.[21,34] In addition, temperature desorption spectroscopy (TDS) analysis was performed for several a-Si:H films to obtain further insight on hydrogen and Si—H bonds within a-Si:H films.

Table 1. Parameters for the growth of intrinsic a-Si:H layers in this study.

Layer	i_1			i_2
Series	Si_2H_6	Temperature	Pressure	–
Si precursor	SiH_4, Si_2H_6	SiH_4	SiH_4	SiH_4
Si_2H_6 concentration, C_{Si2H6} $[Si_2H_6]/([SiH_4]+[Si_2H_6])$	0–75%	0	0	0
Hydrogen dilution $[H_2]/[SiH_4]$	0	0	0	10
Substrate temperature, T_s [°C]	200	30–400	200	200
Pressure, P [Pa]	13, 40	13	13–40	13
Power density [mW cm^{-2}]	11	11	11	11

2.2. SHJ Solar Cells

The intrinsic a-Si:H layers were applied to SHJ solar cells. n-type FZ-Si wafers (P-doped, ≈2Ω cm, <100>-oriented, 280 μm thick) were used as substrates, which were textured to form random pyramids on both surfaces with a KOH-based solution (Hayashi Pure Chemical, Pure Tech). After a wet-chemical cleaning procedure,[27] (i), (p), and (n)-a-Si:H layers were successively deposited on both sides of the textured wafers by means of PECVD. No additional smoothening of the pyramids was applied prior to the a-Si:H deposition. For the i-layer deposition, either single i-layers (i_1-only) or i-bilayers ($i_1 + i_2$) were applied as shown in **Figure 1**. The i-bilayers were grown by a two-step PECVD process: The first interfacial i-layer (i_1) was grown under various conditions, as listed in Table 1, and the second i-layer (i_2) was grown with hydrogen-diluted SiH_4 plasma at a fixed condition. The nominal thicknesses of a-Si:H layers on textured wafers were determined using codeposited films on flat wafers with SE. Therefore, the actual thickness of each layer on a textured wafer was thinner than the nominal value by a factor of ≈0.7.[21] The nominal thicknesses of the i-, p- and n-layers were 10, 5, and 15 nm, respectively. For i-bilayers, the nominal thicknesses of i_1- and i_2-layers were fixed at 2 and 8 nm, respectively, which were determined as an optimum combination in terms of conversion efficiency from previous studies.[21,35]

The effective minority carrier lifetime (τ_{eff}) of the passivated samples was characterized by the quasi-steady-state photoconductance (QSSPC) technique (Sinton Instruments, WCT-120), for quantifying the implied V_{OC} (iV_{OC}). For completing SHJ solar cells, In_2O_3:Sn (ITO) films and Ag electrodes were formed with magnetron sputtering on both sides of the passivated wafer. Prior to Ag sputtering, thermal annealing was performed at 160 °C for 2 h in ambient air. Note that the front metal grid was not optimized, resulting in a relatively large shadow loss and series resistance. The current density–voltage (J–V) characteristics of the fabricated cells were evaluated using a solar

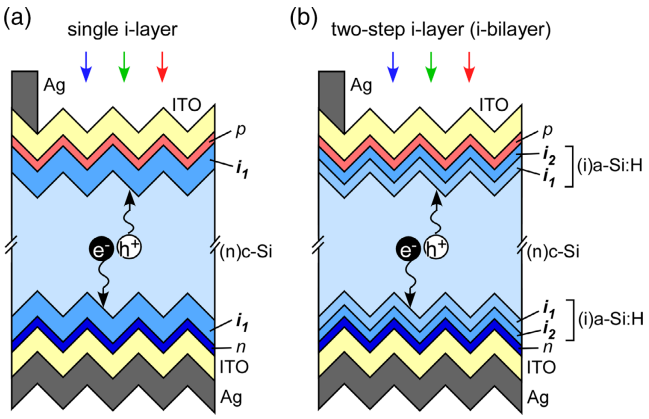

Figure 1. Schematic illustrations of the front-emitter-type SHJ solar cells prepared in this study with a) single i-layers and b) two-step i-layers (i-bilayers).

simulator under air mass 1.5 global (AM 1.5 g) and 100 mW cm^{-2} illumination at 25 °C, and the V_{OC}, the short-circuit current density (J_{SC}), the fill factor (FF), and the conversion efficiency (η) were recorded. All the cells were characterized under illumination from the p-layer side (front-emitter configuration). The cell area was 1.045 cm^2, designated by a shadow mask unless noted otherwise. Light-intensity-dependent V_{OC} measurement (suns-V_{OC}) was also performed to extract the pseudo fill factor (pFF).[36]

3. Results

3.1. Intrinsic a-Si:H Layers

3.1.1. Si—H Bond Structure

PECVD-grown a-Si:H films contain a significant amount of hydrogen, most of which forms Si—H bonds. Such Si-bonded hydrogen can be incorporated in the amorphous network in different manners, e.g., as an isolated Si—H or in the form of hydrogen clusters. In the latter case, Si—H_2 and Si—H_3 are grouped together preferentially at the surface of nanosized voids.[37] IR absorption by Si—H stretching vibration occurs at 2000 cm^{-1} for the isolated Si—H bonds (low-stretching mode, LSM), and at ≈2100 cm^{-1} for the Si—H bonds associated with hydrogen clusters (high-stretching mode, HSM).[34,38–40] **Figure 2** shows the IR absorption spectra of thin a-Si:H films (≈10 nm) grown at different T_S from 30 to 400 °C. All the spectra show absorption due to Si—H bonds in the range of 1900–2200 cm^{-1} depending on T_S. As we did in the previous work,[21] here we simply assign the peaks centered at ≈2000 and ≈2100 cm^{-1} to the LSM and HSM, respectively, although more detailed deconvolution and peak assignments are possible as reported by Burrows et al.[41] The absorption by HSM increases markedly with the decrease in T_S, whereas absorption by LSM decreases slightly. This means that a-Si:H films contain more hydrogen and become more void-rich with the decrease in T_S. Here we use the microstructure factor, R^*, to quantify the Si—H bond microstructure within a-Si:H network. R^* is defined by[31]

$$R^* = I_{HSM}/(I_{LSM} + I_{HSM}) \quad (1)$$

where I_{LSM} and I_{HSM} are the absorption peak intensities of the LSM and HSM in the IR absorption spectra, respectively. They are quantified by curve fitting using Gaussian functions, as shown by the dashed curves in Figure 2. By definition, higher R^* means a greater density of nanosized voids within a-Si:H films. It is confirmed that the R^* of a-Si:H films varies in a wide range from 0.87 to 0.12 by changing the T_S from 30 to 400 °C, as clearly shown in Figure 2. As reported in the previous work, the R^* of a-Si:H films can be controlled also by modifying the gas pressure and the power density during a-Si:H growth.[21] In addition, we confirmed that the R^* can be modified using Si_2H_6 as a precursor gas as well.[35] Furthermore, the R^* can be also controlled by radical separation or filtering during the PECVD process such as by the triode-PECVD technique.[42,43] Thus, Si—H bond structures within the a-Si:H network are affected by various growth parameters.

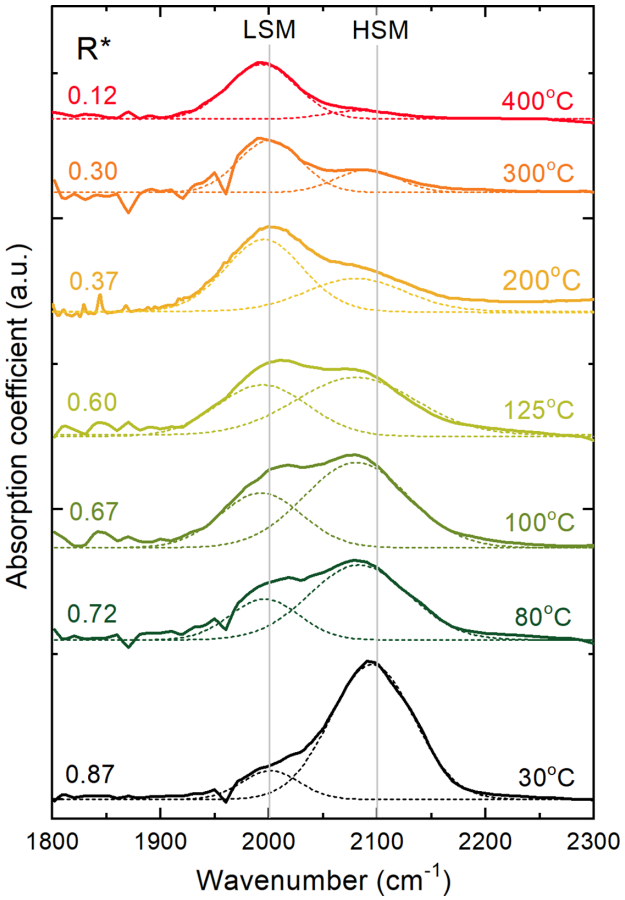

Figure 2. Absorption coefficient spectra of thin a-Si:H films (≈10 nm) grown at different substrate temperatures (T_S) measured with FT-IR. The dashed lines show the fitting results with double Gaussian functions for deconvoluting the HSMs and LSMs.

3.1.2. Material Properties and Microstructure Factor

Here we compare the properties of the a-Si:H films grown under different series of experiments (T_S, P, and C_{Si2H6} series) with respect to R^*. **Figure 3** summarizes the typical parameters of the a-Si:H films prepared in this work, namely, the DR, the n_1, the C_H, and the E_g, as a function of R^*. As shown in Figure 3a, the R^* as well as the DR increased with the increase in P and C_{Si2H6}. In this series, the R^* shows a strong correlation with the DR; i.e., the faster deposition leads to more porous a-Si:H films. The highest DR of ≈1 nm s^{-1} is obtained by combining a high P and a high C_{Si2H6} as plotted by the hexagon in Figure 3a, although the increment of the R^* is limited as it is already close to the maximum (unity). In contrast, the R^* can be controlled independently from the DR by varying the T_S, as shown in the red squares. In this case, migration of adatoms at the growth surface and hydrogen desorption are enhanced by the increase in T_S, resulting in a denser a-Si:H film. The lowest R^* of 0.12 is obtained at $T_S = 400$ °C. The correlation between the R^* and the n_1, which is an index of the film density, is shown in Figure 3b. As a general trend among all data, the n_1 decreases with the increase in R^*, despite the differences in the DR.

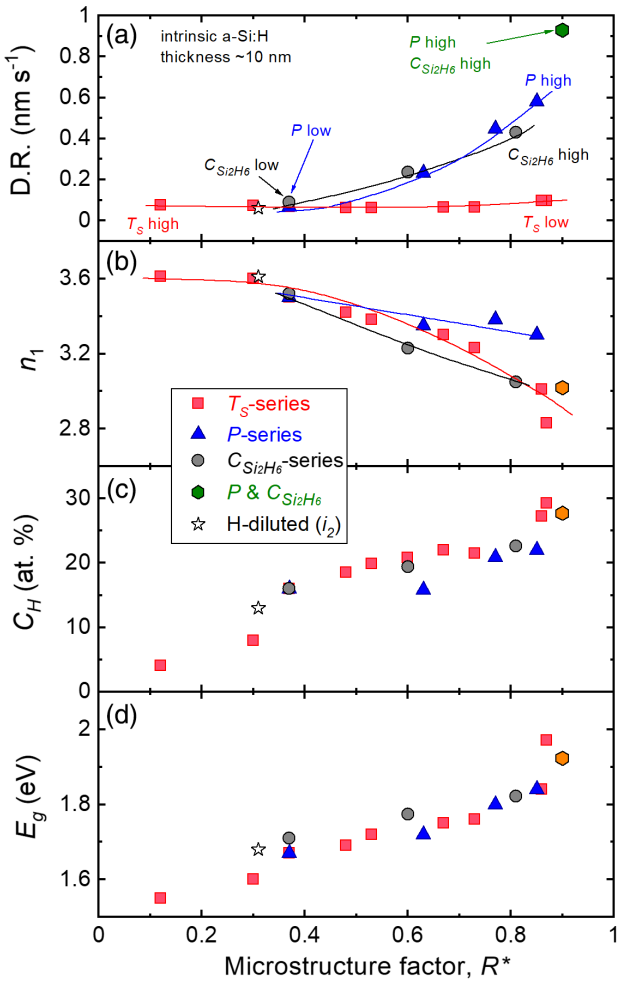

Figure 3. Characteristics of intrinsic a-Si:H thin films grown with PECVD under various conditions, as function of the microstructure factor, R^*: a) the DR, b) the refractive index at 1 eV (n_1), c) the hydrogen concentration (C_H) determined with FT-IR, and d) the energy bandgap (E_g) determined by the Tauc model. The thickness of the a-Si:H films was controlled to be ≈10 nm. The different symbol shapes denote the different series of experiment: T_S series (red square), P series (blue triangle), C_{Si2H6} series (gray circle), a combination of high P and C_{Si2H6} (orange hexagon). The star symbol denotes the H-dilution condition, which is used as the i_2-layer in this work. The numbers next to the plots in (a) indicate the corresponding values of the T_S, P, and C_{Si2H6}. The solid lines are guides to the eye.

However, it is found that the n_1 of the P series is slightly higher than those of the T_S and C_{Si2H6} series in the range of $R^* > 0.7$. This suggests a possibility to control the n_1 and the R^* independently to some extent. In contrast, the C_H and the E_g of a-Si:H films increase monotonically with the increase in R^*, as shown in Figure 3c,d, respectively. Here the C_H is calculated from the absorption spectra obtained by FT-IR spectroscopy.[21,34] The C_H increases significantly from 4 to 30 at% with the increase in R^*. This is mainly attributed to the drastic increase in the Si—H bond density associated with HSM, as confirmed in Figure 2 for the T_S series. The E_g increases from 1.55 to almost 2 eV with the increase in R^*, which can be explained by the well-known positive correlation with the E_g and the C_H of a-Si:H film.[37] In these graphs, the data of a-Si:H film grown with hydrogen-diluted plasma (SiH_4:H_2 = 1:10) are included as an open star symbol for reference. This relatively dense a-Si:H film with E_g = 1.7 eV and C_H = 13% will be used as the i_2-layer in the following sections.

The different natures of Si—H bonds within a-Si:H films with different R^* are also confirmed by TDS analysis, as shown in **Figure 4**. In this graph, the H_2 effusion rates of two a-Si:H films (R^* = 0.37 and 0.82) are compared as representatives of low- and high-R^* films. The low-temperature peak β represents the desorbed H_2 from ruptured Si—H bonds at internal voids and interfaces,[44–46] which are assigned to the HSM. The high-temperature peak α represents the desorbed H_2 from the rupture of Si—H bonds related to the LSM, and the trapped molecular H_2 in nanosized voids.[47] As the R^* increases, the β peak shifts to lower temperature and the peak intensity increases. This indicates that the a-Si:H film with high R^* contains a high density of weak S—H bonds (probably in forms of $Si—H_2$ and $Si—H_3$), which are easily ruptured at low temperatures. In addition, the slightly decreased α peak is probably ascribed to the lower density of monohydride bonds. In TDS analysis, we can quantify the total hydrogen content, C_{H_total}, including hydrogen molecules incorporated within a-Si:H films without forming Si—H bonds. For the a-Si:H films with R^* = 0.37 and 0.82, we obtain C_{H_total} = 20.2% and 23.9%, respectively, which are slightly higher than their C_H determined by FT-IR (15.9% and 22.5%, respectively). It is revealed that the gap between C_{H_total} and C_H, i.e., the amount of hydrogen molecules trapped within a-Si:H films, decreases with the increase in R^*. This result might suggest that hydrogen molecules easily escape from a-Si:H films with high R^* during the film growth.

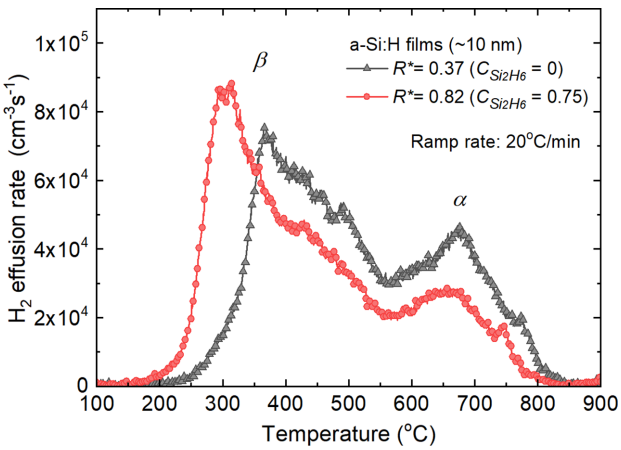

Figure 4. Hydrogen effusion rates from thin a-Si:H layers with different R^*. The thickness of the films is controlled to ≈10 nm, and the films are heated from room temperature to 900 °C with a ramping rate of 20 °C min^{-1}.

3.2. Surface Passivation and Photovoltaic Performance in SHJ Cells

3.2.1. SHJ Cells with Single i-Layers

In the following sections, we move our focus on to the effects of various i-layers on the photovoltaic parameters in SHJ solar cells. First, we investigate the photovoltaic parameters of SHJ solar cells that have single i-layers for surface passivation, as shown in Figure 1a. **Figure 5** summarizes the solar cell results as a function of R^* of the i-layer. In this figure, we use the R^* determined in Figure 3 on planer wafers in the horizontal axis. The nominal thicknesses of all the i-layers were controlled to ≈10 nm. Note that the condition showing the highest DR in Figure 2a was not applied here due to the difficulty in precise control of thickness. As shown in Figure 5a, the J_{SC} does not depend on either the growth conditions or the R^* of the i-layers, although those of the T_S series show slightly lower values than the others. In contrast, the V_{OC} depends largely on the R^* and shows different behaviors for each series of experiment, as shown in Figure 5b. In the case of the T_S series, the V_{OC} first increases with the increase in R^* and takes the maximum at $R^* \approx 0.4$. This can be attributed to the improved surface passivation due to the mitigation of epitaxial growth at the a-Si:H/c-Si interface because epitaxial growth occurs more easily with the increase in T_S.[16,48] However, further increase in R^* leads to the decrease in V_{OC} probably due to the deteriorated surface passivation by using more porous and defective a-Si:H films. The decrease in V_{OC} with the increase in R^* is also found in the P and C_{Si2H6} series, which is ascribable to the same mechanisms. The maximum V_{OC} obtained here is limited below 0.70 V, which is rather low for SHJ solar cells. In addition, using the 10 nm thick i_2-layer (H-dilution condition) as a single i-layer for passivation does not improve the V_{OC} as plotted with the star symbol. These results indicate that surface passivation of c-Si wafers with single i-layers is not straightforward. The iV_{OC} shows slightly higher values than the V_{OC}, but the trend is very similar. The poor surface passivation by the single i-layers is also confirmed by the low pFF values (<0.81), as shown in Figure 5c, although it increases slightly with the increase in R^*. The gap between the pFF and the FF, which is attributable to the series resistance loss within the cells, is found to be almost constant for the P and the C_{Si2H6} series. However, the gap increases for the T_S series with the increase in R^*, i.e., with the decrease in T_S. This result reveals that the series resistance loss increases on lowering the T_S, probably due to the reduction in the electrical conductivity of a-Si:H layers. Overall, the η is governed by the V_{OC} as shown in Figure 5d. The maximum η obtained here is limited at ≈20% due to the poor surface passivation at the a-Si:H/c-Si interface.

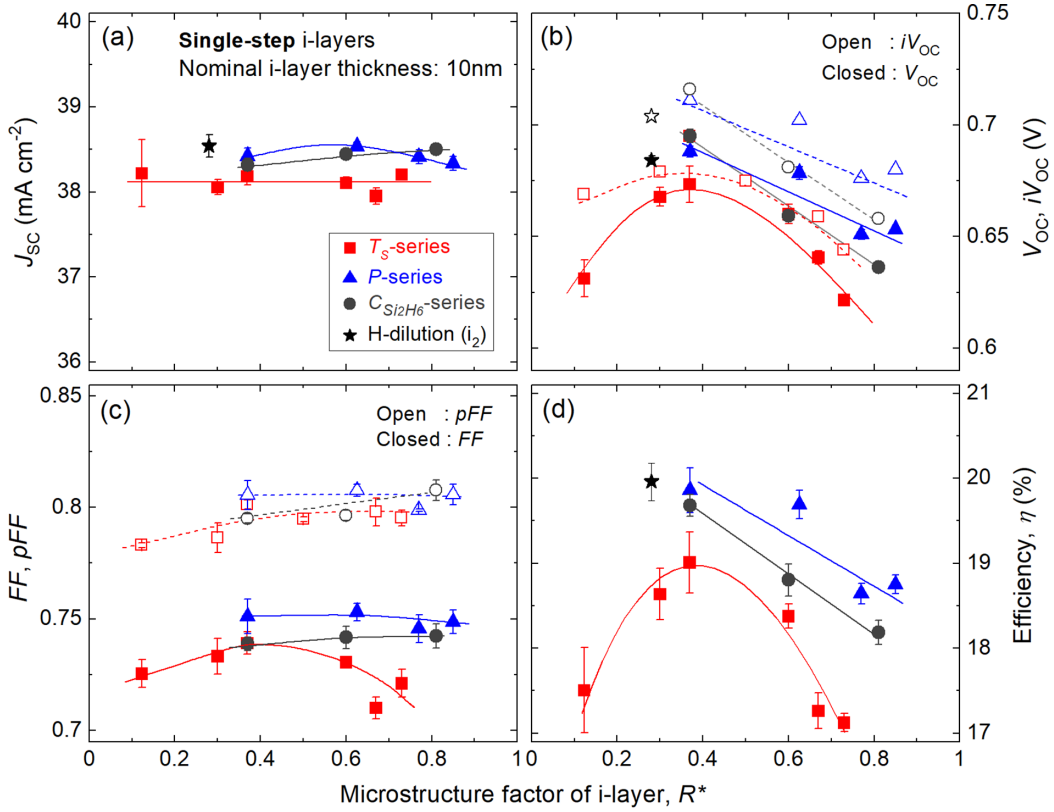

Figure 5. Photovoltaic parameters of SHJ solar cells with single i-layers as a function of R^* of the i-layer: a) J_{SC}, b) iV_{OC} and V_{OC}, c) pFF and FF, and d) conversion efficiency. All the values except iV_{OC} are averaged values of more than eight small area cells (1.045 cm^2) for each condition and the error bars indicate the standard deviation, whereas the iV_{OC} was measured before metallization. The difference in symbol shapes corresponds to the different series of experiments (see the legends). The nominal thicknesses of all the i-layers in the cells are controlled to 10 nm. The solid and dashed lines are guides to the eye.

3.2.2. Improved Surface Passivation by Intrinsic Bilayers

The surface passivation at the a-Si:H/c-Si interface is improved significantly by applying two-step PECVD for the growth of a-Si:H i-layers. **Figure 6** shows the τ_{eff} of passivated wafers with i/N/i and p/i/N/i/n structures (N denotes n-type c-Si wafer) as a function of R^* of i_1-layers. Here we control the R^* of i_1-layers by modifying C_{Si2H6} and compare the following two cases: 1) single i_1-layer (10 nm) and 2) a stack of i_1- and i_2-layers (2 + 8 nm). Note that the R^* in this graph were determined using 10 nm thick i_1-layers, as plotted in Figure 2. As shown inFigure 6, the τ_{eff} is drastically improved by applying the bilayer structure. The τ_{eff} of the passivated wafers with single i-layers (i_1/N/i_1) remains at a rather low level, and it decreases steeply with the increase in R^*. This trend is maintained even after the p- and n-layer deposition (p/i_1/N/i_1/n). These results indicate that the usage of only porous a-Si:H layers is not effective to passivate c-Si surfaces, which is consistent with the results shown in Figure 5b,c. In contrast, the τ_{eff} is improved significantly by applying the bilayers (i_2i_1/N/i_1i_2), and it increases gradually with the increase in R^*. The τ_{eff} decreases to some extent after capping with doped layers (p/i_2i_1/N/i_1i_2/n), but still remains at a high level (>several milliseconds). Interestingly, the best τ_{eff} for the bilayer samples is obtained by using the i_1-layer with the highest R^*, which gives the lowest τ_{eff} in the case of the single-layer passivation.

3.2.3. SHJ Cells with Intrinsic Bilayers

The application of an intrinsic bilayer with a porous interfacial i_1-layer is effective in improving the V_{OC} and the η of SHJ solar cells due to the improved surface passivation. **Figure 7** shows the photovoltaic properties of SHJ solar cells with intrinsic bilayers ($i_1 + i_2 = 2 + 8$ nm), as a function of the R^* of the interfacial i_1-layers. Note that the R^* values in the horizontal axis are determined using 10 nm thick i_1-layers as used in Figure 5. The benefits of using intrinsic bilayers are highlighted by

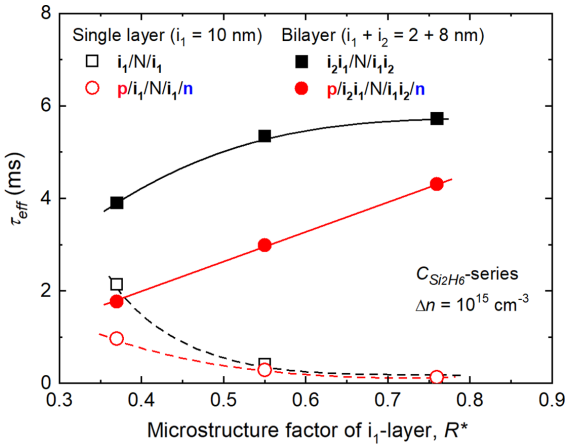

Figure 6. Effective minority carrier lifetime τ_{eff} of textured Si wafers passivated with a-Si:H layers (single layers or bilayers) as a function of the microstructure factor of the i_1-layer, R^*. The R^* values in the horizontal axis are determined using 10 nm thick i_1-layers and modified by adjusting the C_{Si2H6} in the PECVD process. The τ_{eff} were measured at the minority carrier density of $\Delta n = 1 \times 10^{15}$ cm^{-3}.

comparing Figure 5 and 7. It is clearly confirmed that the V_{OC} as well as the iV_{OC} is markedly improved by using the intrinsic bilayers as shown in Figure 7b regardless of the series of experiments. The V_{OC} increases gradually with the increase in R^*, except for the highest R^* in the T_S-series. The maximum V_{OC} as well as the maximum iV_{OC} is obtained in the C_{Si2H6} series at $R^* \approx 0.8$, which is attributed to the improved surface passivation, as confirmed in Figure 6. However, it is also found that a high i$V_{OC} \approx 0.725$ V ($V_{OC} > 0.70$ V) is attainable even in the T_S and P series at $R^* = 0.7$–0.8. The effect of the improved surface passivation can be confirmed also in the behaviors of the pFF, as shown in Figure 7c. The pFF is improved by using intrinsic bilayers up to 0.825 at $R^* = 0.7$–0.8, which is ≈0.02 higher than that obtained with single i-layers. In addition, the FF in the T_S series is largely enhanced by using bilayers, which is attributable to the improved electrical conductivity. However, the maximum FF obtained here remains at a moderate level (≈0.76) because it is still limited by the series resistance losses. In contrast to the V_{OC} and FF, the J_{SC} shows rather minor dependence on R^*, which is similar to that of the single i-layer case shown in Figure 5a. Overall, the η is largely improved by using intrinsic bilayers,as shown in Figure 7d. The best efficiencies close to 21% are obtained at $R^* = 0.7$–0.8 due to the improvements in the V_{OC} and the FF, regardless of the series of experiments. From these results, it is concluded that the i-bilayer configuration with a porous interfacial layer is effective in improving surface passivation at the a-Si:H/c-Si interface and enhancing the efficiency of SHJ solar cells, and that various process parameters in the PECVD process (temperature, pressure, or precursor gas species) can be utilized to grow the interfacial layer if its R^* is controlled within a proper range. Needless to say, the most convenient and cost-effective parameter should be chosen to control R^* from the industrial point of view.

We performed further fine-tuning of the intrinsic bilayer together with enlarging the cell size from 1 to 4 cm^2 and replacing our standard ITO with a more transparent W and H codoped In_2O_3 (In_2O_3:W, H) film.[49] As a result, the η of our SHJ cell was improved from 21% to 23.0%, as shown in **Figure 8**. Here, the intrinsic bilayer used in this cell has the same structure as that used in Figure 7 ($i_1 + i_2 = 2 + 8$ nm), and the R^* of the i_1-layer was controlled to ≈0.8 by modifying the pressure and the power density in the PECVD process. Note that the V_{OC} of this cell (0.724 V) is lower than those of record cells (>0.740 V in many cases), mainly due to the large thickness of the wafer (270 μm) and the small cell area (4 cm^2).

4. Discussions

4.1. Role of Interfacial Porous a-Si:H Layer

The R^* of the i_1-layer in the intrinsic bilayer is closely correlated to the surface passivation properties at the a-Si:H/c-Si interface, particularly after the deposition of overlying doped-layers, as confirmed in Figure 6. According to the results shown in Figure 3 and 4, a-Si:H films become more porous and H-rich with an increase in R^*, which is more effective to prevent epitaxial growth at the a-Si:H/c-Si interface. However, such a porous interfacial layer itself is not effective to terminate dangling bonds

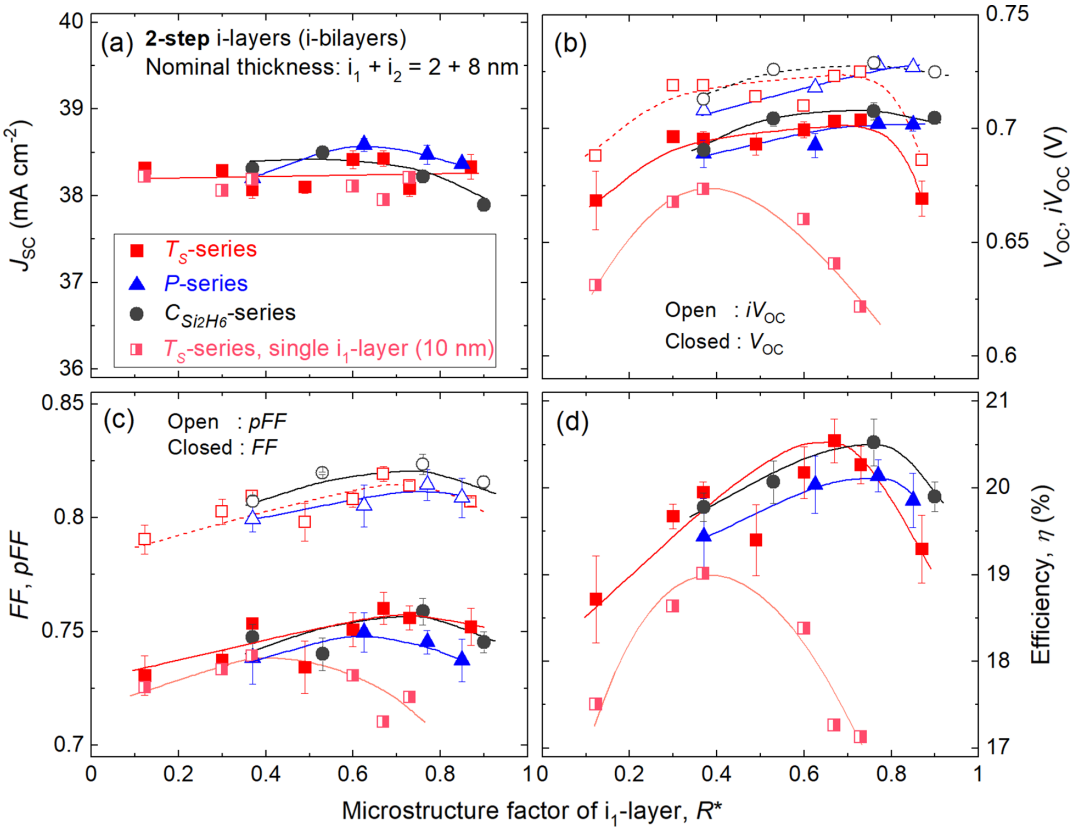

Figure 7. Photovoltaic parameters of SHJ solar cells with intrinsic bilayers as a function of R^* of the i_1-layer: a) J_{SC}, b) iV_{OC}, and V_{OC}, c) pFF and FF, and d) conversion efficiency. All the values except iV_{OC} are averaged values of more than eight small area cells (1.045 cm^2) and the error bars indicate the standard deviation, whereas the iV_{OC} was measured before metallization. The difference in symbol shapes corresponds to the different series of experiments (see the legends). For comparison, the T_S series with single i_1 layers is also plotted with half-filled squares. Note that the R^* values in the horizontal axis are determined using 10 nm thick i_1-layers. The solid and dashed lines are guides to the eye.

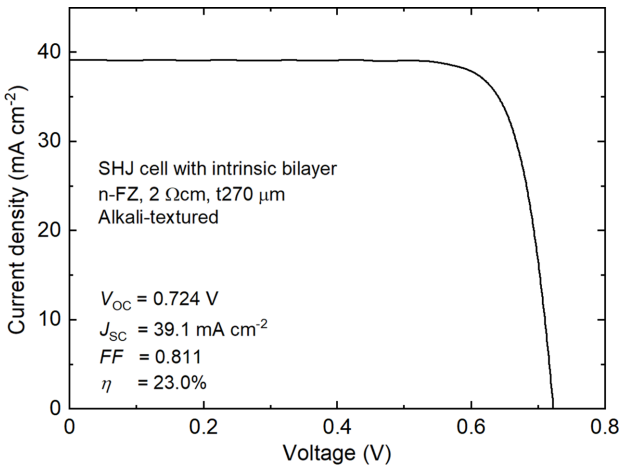

Figure 8. Current density–voltage curve of the best-performing SHJ solar cell fabricated in this work. The optimized intrinsic bilayer was applied for surface passivation. The cell area is designated at 4.0 cm^2 with a shadow mask. In this cell, an In_2O_3:W, H film is applied as a front window layer instead of our standard ITO. No additional antireflection coating is applied.

on the c-Si surface, as shown inFigure 5, and therefore an overlying dense a-Si:H layer is required for better surface passivation, as shown in Figure 6. Generally, dense a-Si:H layers are grown with H-diluted plasma, which often causes partial crystallization, whereas porous a-Si:H layers can be grown with SiH_4 (or mixed with Si_2H_6) plasmas without H dilution (or with minimal H dilution). It is known that H radicals in H-rich plasmas can penetrate into c-Si bulk and generate defects, which can work as recombination centers.[50,51] The formation of defective regions within c-Si underneath a-Si:H layers was confirmed by transmission electron microscope observations.[4,21,51] In addition, the advantage of using pure SiH_4 plasma for mitigating the plasma-induced defects within c-Si was also confirmed by in situ photocurrent measurements with Si-on-insulator (SOI) wafers.[18] The deposition of a porous a-Si:H layer without H dilution is expected to be effective to protect the c-Si absorber from direct exposure to H-diluted plasmas and defect formation by H radicals. Thus, the interfacial i-layer has two roles: as a buffer layer for preventing the epitaxial growth at the a-Si:H/c-Si interface and as a protection layer from H radicals within H-diluted plasmas, which is necessary to grow a dense a-Si:H layer for surface passivation.

It is known that the microstructure of a-Si:H thin layers is reorganized by the post-H_2-plasma treatment.[52,53] In the bilayer configuration used in this work, the reorganization of the interfacial i_1-layer must occur during the overlying i_2-layer deposition with a H-diluted plasma. This means that the i_1-layer in the as-deposited state could be an intermediate state and different from that in the completed cell. Detailed analysis of the reorganization remains as a future work. All of the PECVD process must be optimized for realizing the best surface passivation in the completed cell. Nevertheless, the R^* of as-deposited i_1-layers is a very useful parameter as the R^* of bilayers is dominated by the i_2-layers and the footprints of the i_1-layers are mostly hidden.

4.2. Impact of i_1-Layer on Series Resistance

If we focus only on surface passivation, it is possible to use a thicker (>2 nm) interfacial a-Si:H layer in the bilayer structure. In fact, the best τ_{eff} was obtained when using a 4 nm thick interfacial layer in the previous report.[21] However, it was also found in the previous report that the FF of SHJ solar cells is deteriorated with the increase in R^* of the interfacial a-Si:H layer, which is ascribed to the increase in series resistance.[21] Thus, R^* must be tuned to balance surface passivation and carrier transport in SHJ solar cells. In this respect, the interfacial layer with high R^* should be as thin as possible. There may be room for improvement in the series resistance loss by reducing the i_1-layer thickness because we fixed it at 2 nm in this work. This will be a topic of our future work. It is worth noting that very thin interfacial layers (0.5–1 nm) were applied in the record-efficiency SHJ cell.[4] In addition, it would be beneficial to increase the density of the interfacial layer from the viewpoint of carrier transport, although its R^* must be controlled within a proper range to impede epitaxial growth and maintain superior surface passivation.

5. Conclusion

In this study, we investigated the impact of intrinsic a-Si:H bilayers, composed of a porous interfacial layer and a dense layer, on the photovoltaic performance in SHJ solar cells. We prepared a-Si:H layers with a wide range of film densities and hydrogen contents by modifying various PECVD parameters such as substrate temperature, pressure, and gas species, including Si_2H_6. The a-Si:H films prepared in this work displayed poor surface passivation when applied as a single i-layer. However, surface passivation at the a-Si:H/c-Si interface was significantly improved by applying bilayers. In the case of the bilayer configuration, the microstructure factor R^* of the interfacial layer is a good measure for achieving good surface passivation; using an interfacial layer with high R^* (0.7–0.8) leads to better surface passivation, and therefore the enhancements of the V_{OC} and the conversion efficiency in SHJ cells. Interestingly, various process parameters in the PECVD process (temperature, pressure, and precursor gas species) can be utilized to grow an effective interfacial layer if its R^* is controlled within a suitable range. This indicates that R^* is a key universal parameter to develop the growth process of the interfacial a-Si:H layer for high-efficiency SHJ solar cells. In addition, the interfacial layer should be as thin as possible because it causes an increase in the series resistance.

Acknowledgements

The authors acknowledge T. Oku, Y. Sato, and M. Tanabe for technical support in this work, T. Koida for the deposition of In_2O_3:W, H films, and C. McDonald for the fruitful discussion. A part of this work was conducted under a project commissioned by the New Energy and Industrial Technology Development Organization (NEDO), Japan.

Conflict of Interest

The authors declare no conflict of interest.

Data Availability Statement

Research data are not shared.

Keywords

amorphous silicon, Fourier transform infrared spectroscopy, heterojunctions, hydrogen, plasma chemical vapor deposition, silicon solar cells, surface passivation

Received: November 24, 2020
Revised: February 16, 2021
Published online: March 6, 2021

[1] M. Tanaka, M. Taguchi, T. Matsuyama, T. Sawada, S. Tsuda, S. Nakano, H. Hanafusa, Y. Kuwano, *Jpn. J. Appl. Phys.* **1992**, *31*, 3518.
[2] S. De Wolf, A. Descoeudres, Z. C. Holman, C. Ballif, *Green* **2012**, *2*, 7.
[3] D. Adachi, J. L. Hernández, K. Yamamoto, *Appl. Phys. Lett.* **2015**, *107*, 233506.
[4] X. Ru, M. Qu, J. Wang, T. Ruan, M. Yang, F. Peng, W. Long, K. Zheng, H. Yan, X. Xu, *Sol. Energy Mater. Sol. Cells* **2020**, *215*, 110643.
[5] K. Masuko, M. Shigematsu, T. Hashiguchi, D. Fujishima, M. Kai, N. Yoshimura, T. Yamaguchi, Y. Ichihashi, T. Mishima, N. Matsubara, T. Yamanishi, T. Takahama, M. Taguchi, E. Maruyama, S. Okamoto, *IEEE J. Photovoltaics* **2014**, *4*, 1433.
[6] K. Yoshikawa, W. Yoshida, T. Irie, H. Kawasaki, K. Konishi, H. Ishibashi, T. Asatani, D. Adachi, M. Kanematsu, H. Uzu, K. Yamamoto, *Sol. Energy Mater. Sol. Cells* **2017**, *173*, 37.
[7] M. Taguchi, A. Yano, S. Tohoda, K. Matsuyama, Y. Nakamura, T. Nishiwaki, K. Fujita, E. Maruyama, *IEEE J. Photovoltaics* **2014**, *4*, 96.
[8] H. Sai, T. Oku, Y. Sato, M. Tanabe, T. Matsui, K. Matsubara, *Prog. Photovoltaics Res. Appl.* **2019**, *27*, 1061.
[9] A. Danel, S. Harrison, F. Gerenton, A. Moustafa, R. Varache, J. Veirman, C. Roux, in *Proc. 35th EUPVSEC*, WIP-Renewable Energies, Munich **2018**, pp. 444–447.
[10] A. Augusto, J. Karas, P. Balaji, S. G. Bowden, R. R. King, *J. Mater. Chem. A* **2020**, *8*, 16599.
[11] T. Mishima, M. Taguchi, H. Sakata, E. Maruyama, *Sol. Energy Mater. Sol. Cells* **2011**, *95*, 18.
[12] A. Bianchini, M. Gambuti, M. Pellegrini, C. Saccani, *Renewable Energy* **2016**, *85*, 1.
[13] J. Haschke, J. P. Seif, Y. Riesen, A. Tomasi, J. Cattin, L. Tous, P. Choulat, M. Aleman, E. Cornagliotti, A. Uruena, R. Russell, F. Duerinckx, J. Champliaud, J. Levrat, A. A. Abdallah, B. Aïssa, N. Tabet, N. Wyrsch, M. Despeisse, J. Szlufcik, S. De Wolf, C. Ballif, *Energy Environ. Sci.* **2017**, *10*, 1196.
[14] H. Fujiwara, M. Kondo, *J. Appl. Phys.* **2007**, *101*, 1.
[15] S. De Wolf, A. Descoeudres, Z. C. Holman, C. Ballif, *Green* **2012**, *2*, 7.

[16] H. Fujiwara, M. Kondo, *Appl. Phys. Lett.* **2007**, *90*, 013503.
[17] S. De Wolf, M. Kondo, *Appl. Phys. Lett.* **2007**, *90*, 042111.
[18] S. Nunomura, I. Sakata, H. Sakakita, K. Koga, M. Shiratani, *J. Appl. Phys.* **2020**, *128*, 033302.
[19] W. Liu, L. Zhang, R. Chen, F. Meng, W. Guo, J. Bao, Z. Liu, *J. Appl. Phys.* **2016**, *120*, 175301.
[20] Y. Zhang, C. Yu, M. Yang, L.-R. Zhang, Y.-C. He, J.-Y. Zhang, X.-X. Xu, Y.-Z. Zhang, X.-M. Song, H. Yan, *Chin. Phys. Lett.* **2017**, *34*, 038101.
[21] H. Sai, P. W. Chen, H. J. Hsu, T. Matsui, S. Nunomura, K. Matsubara, *J. Appl. Phys.* **2018**, *124*, 103102.
[22] H. Fujiwara, T. Kaneko, M. Kondo, *Appl. Phys. Lett.* **2007**, *91*, 5.
[23] K. Ding, U. Aeberhard, F. Finger, U. Rau, *J. Appl. Phys.* **2013**, *113*, 134501.
[24] M. Boccard, Z. C. Holman, *J. Appl. Phys.* **2015**, *118*, 065704.
[25] W. Liu, F. Meng, X. Zhang, Z. Liu, *ACS Appl. Mater. Interfaces* **2015**, *7*, 26522.
[26] K. Ohdaira, T. Oikawa, K. Higashimine, H. Matsumura, *Curr. Appl. Phys.* **2016**, *16*, 1026.
[27] S. N. Granata, T. Bearda, F. Dross, I. Gordon, J. Poortmans, R. Mertens, *Energy Procedia* **2012**, *27*, 412.
[28] D. Deligiannis, R. Vasudevan, A. H. M. Smets, R.A.C.M.M. van Swaaij, M. Zeman, *AIP Adv.* **2015**, *5*, 097165.
[29] S. De Wolf, M. Kondo, *Appl. Phys. Lett.* **2007**, *91*, 112109.
[30] J. P. Seif, B. Niesen, A. Tomasi, C. Ballif, S. De Wolf, *Appl. Phys. Lett.* **2017**, *110*, 151601.
[31] J. Müllerová, P. Šutta, G. van Elzakker, M. Zeman, M. Mikula, *Appl. Surf. Sci.* **2008**, *254*, 3690.
[32] A. Matsuda, T. Kaga, H. Tanaka, L. Molhotra, K. Tanaka, *Jpn. J. Appl. Phys.* **1983**, *2*, L115.
[33] H. T. Chen, H. W. Huang, *J. Phys. Chem. C* **2014**, *118*, 20314.
[34] A. A. Langford, M. L. Fleet, B. P. Nelson, W. A. Lanford, N. Maley, *Phys. Rev. B* **1992**, *45*, 13367.
[35] P. W. Chen, P. L. Chen, H. J. Hsu, T. Matsui, H. Sai, C. C. Tsai, K. Matsubara, in *2018 IEEE 7th World Conf. Photovolt. Energy Conversion, WCPEC 2018 – A Jt. Conf. 45th IEEE PVSC, 28th PVSEC 34th EU PVSEC 1982*, IEEE, New York, NY, USA **2018**.
[36] R. Sinton, A. Cuevas, in *16th Eur. Photovolt. Sol. Energy Conf.*, Routledge (Taylor & Francis Group), Glasgow **2000**, pp. 1–4.
[37] W. Beyer, in *Thin Film Silicon Solar Cells* (Ed: A. Shah), EPFL Press, Lausanne **2010**, pp. 64–76.
[38] M. H. Brodsky, M. Cardona, J. J. Cuomo, *Phys. Rev. B* **1977**, *16*, 3556.
[39] G. Lucovsky, *Sol. Cells* **1980**, *2*, 431.
[40] A. H. M. Smets, W. M. M. Kessels, M. C. M. van de Sanden, *Appl. Phys. Lett.* **2003**, *82*, 1547.
[41] M. Z. Burrows, U. K. Das, R. L. Opila, S. De Wolf, R. W. Birkmire, *J. Vac. Sci. Technol., A* **2008**, *26*, 683.
[42] H. Sonobe, A. Sato, S. Shimizu, T. Matsui, M. Kondo, A. Matsuda, *Thin Solid Films* **2006**, *502*, 306.
[43] T. Matsui, H. Sai, K. Saito, M. Kondo, *Prog. Photovoltaics Res. Appl.* **2013**, *21*, 1363.
[44] N. Yabumoto, K. Saito, M. Morita, *Jpn. J. Appl. Phys.* **1991**, *30*, L419.
[45] W. Beyer, H. Wagner, *J. Non-Cryst. Solids* **1983**, *59–60*, 161.
[46] D. K. Biegelsen, R. A. Street, C. C. Tsai, J. C. Knights, *Phys. Rev. B* **1979**, *20*, 4839.
[47] W. Beyer, H. Wagner, J. Chevallier, K. Reichelt, *Thin Solid Films* **1982**, *90*, 145.
[48] J. J. H. Gielis, P. J. Van Den Oever, B. Hoex, M. C. M. Van De Sanden, W. M. M. Kessels, *Phys. Rev. B* **2008**, *77*, 1.
[49] T. Koida, J. Nishinaga, Y. Ueno, H. Higuchi, H. Takahashi, M. Iioka, Y. Kamikawa, H. Shibata, S. Niki, *Prog. Photovoltaics Res. Appl.* **2019**, *27*, 491.
[50] S. J. Jeng, G. S. Oehrlein, G. J. Scilla, *Appl. Phys. Lett.* **1988**, *53*, 1735.
[51] J. Geissbühler, S. De Wolf, B. Demaurex, J. P. Seif, D. T. L. Alexander, L. Barraud, C. Ballif, *Appl. Phys. Lett.* **2013**, *102*, 231604.
[52] A. Descoeudres, L. Barraud, S. De Wolf, B. Strahm, D. Lachenal, C. Guérin, Z. C. Holman, F. Zicarelli, B. Demaurex, J. Seif, J. Holovsky, C. Ballif, *Appl. Phys. Lett.* **2011**, *99*, 123506.
[53] J. Shi, M. Boccard, Z. Holman, *Appl. Phys. Lett.* **2016**, *109*, 031601.